This Accepted Manuscript has not been copyedited and formatted. The final version may differ from this version.

eNeuro

Research Article: New Research | Disorders of the Nervous System

Efficient Remyelination Requires DNA Methylationxs

DNA methylation in remyelination

Sarah Moyon[1,*], Dan Ma[4,*], Jimmy L. Huynh[1,2], David J.C. Coutts[4], Chao Zhao[4], Patrizia Casaccia[1,2,3] and Robin J. M. Franklin[4]

[1]*Department of Neuroscience, Icahn School of Medicine at Mount Sinai, New York, NY 10029, USA*

[2]*Department of Genetics and Genomic Sciences, Icahn School of Medicine at Mount Sinai, New York, NY 10029, USA*

[3]*Neuroscience Initiative Advanced Science Research Center, CUNY, 85 St Nicholas Terrace, New York, NY 10031*

[4]*Wellcome Trust-Medical Research Council Cambridge Stem Cell Institute and Department of Clinical Neurosciences, University of Cambridge, Cambridge, CB2 0AH, UK*

DOI: 10.1523/ENEURO.0336-16.2017

Received: 7 November 2016

Revised: 28 January 2017

Accepted: 31 January 2017

Published: 20 March 2017

Author contributions: PC and RJMF designed the research; DM, SM, JLH, DJJC and CZ performed the research; DM, SM, CZ, PC and RJMF analyzed the data; SM wrote the paper with input from other authors.

Funding: NIH
NIH-R37NS42925-14

Funding: NIH
NIH-F31NS077504

Funding: UK Multiple Sclerosis Society

Funding: Paralyzed Veterans of America Research Foundation (PVA Research Foundation)
100001810
3061

Funding: National Multiple Sclerosis Society (National MS Society)
100000890
FG-1507-04996

The authors declare no competing financial interests.

NIH [NIH-R37NS42925-14]; UK Multiple Sclerosis Society

S.M. and D.M. are Co-first authors

Correspondence should be addressed to either Sarah Moyon, Email: sarah.moyon@mssm.edu or Robin J. M. Franklin, rjf1000@cam.ac.uk

Cite as: eNeuro 2017; 10.1523/ENEURO.0336-16.2017

Alerts: Sign up at eneuro.org/alerts to receive customized email alerts when the fully formatted version of this article is published.

Accepted manuscripts are peer-reviewed but have not been through the copyediting, formatting, or proofreading process.

This is an open-access article distributed under the terms of the Creative Commons Attribution 4.0 International (http://creativecommons.org/licenses/by/4.0), which permits unrestricted use, distribution and reproduction in any medium provided that the original work is properly attributed.

Copyright © 2017 the authors

eNeuro Accepted Manuscript

eNeuro Accepted Manuscript

1 **Efficient remyelination requires DNA methylation**

2 *Abbreviated title:* DNA methylation in remyelination

3

4 Sarah Moyon[1,*,#], Dan Ma[4,*], Jimmy L. Huynh[1,2], David J.C. Coutts[4], Chao Zhao[4], Patrizia
5 Casaccia[1,2,3] and Robin J. M. Franklin[4,#]
6
7 [1]Department of Neuroscience
8 [2]Department of Genetics and Genomic Sciences
9 Icahn School of Medicine at Mount Sinai, New York, NY 10029, USA
10 [3]Neuroscience Initiative Advanced Science Research Center, CUNY, 85 St Nicholas Terrace,
11 New York, NY 10031
12 [4]Wellcome Trust-Medical Research Council Cambridge Stem Cell Institute and Department of
13 Clinical Neurosciences, University of Cambridge, Cambridge CB2 0AH, UK
14 * Co-first authors
15 **# Corresponding authors:** sarah.moyon@mssm.edu, rjf1000@cam.ac.uk

16

17 **Author contributions**

18 PC and RJMF designed the research; DM, SM, JLH, DJJC and CZ performed the research;
19 DM, SM, CZ, PC and RJMF analyzed the data; SM wrote the paper with input from other
20 authors.

21

22 **Number of figures:** 5

23 **Number of words:** Abstract (225), Significant statement (95), Introduction (423), Discussion
24 (880)

25

26 **Acknowledgements**

27 This work was supported by NIH-R37NS42925-14 to PC, NIH-F31NS077504 Fellowship to JLH,
28 postdoctoral fellowships from the Paralyzed Veterans of America (3061) and National Multiple
29 Sclerosis Society (FG-1507-04996) to SM, a programme grant from the UK Multiple Sclerosis
30 Society (RJMF, CZ) and a core support grant from the Wellcome Trust and MRC to the
31 Wellcome Trust – Medical Research Council Cambridge Stem Cell Institute (RF).

32

33 **Conflict of Interest**

34 The authors declare no competing financial interests.

eNeuro Accepted Manuscript

35 **Abstract**

36 Oligodendrocyte progenitor cells (OPC) are the principal source of new myelin in the
37 central nervous system and a better understanding of how they mature into myelin-forming cells
38 is of high relevance for remyelination. It has recently been demonstrated that during
39 developmental myelination, the DNA methyltransferase 1 (DNMT1), but not DNMT3A, is critical
40 for regulating proliferation and differentiation of OPC into myelinating oligodendrocytes (OL).
41 However, it remains to be determined whether DNA methylation is also critical for the
42 differentiation of adult OPC during remyelination. After lysolecithin-induced demyelination in the
43 ventrolateral spinal cord white matter of adult mice of either sex, we detected increased levels of
44 DNA methylation and higher expression levels of the DNA methyltransferase DNMT3A and
45 lower levels of DNMT1 in differentiating adult OL. To functionally assess the role of DNMT1 and
46 DNMT3 in adult OPC, we used mice with inducible and lineage-specific ablation of *Dnmt3a*
47 and/or *Dnmt1* (i.e., *Plp-creER(t);Dnmt3a-flox*, *Plp-creER(t);Dnmt1-flox, Plp-creER(t);Dnmt1-*
48 *flox;Dnmt3a-flox*). Upon lysolecithin injection in the spinal cord of these transgenic mice, we
49 detected defective OPC differentiation and inefficient remyelination in the *Dnmt3a* null and
50 *Dnmt1/Dnmt3a* null mice, but not in the *Dnmt1* null mice. Taken together with previous results in
51 the developing spinal cord, these data suggest an age-dependent role of distinct DNA
52 methyltransferases in the oligodendrocyte lineage, with a dominant role for DNMT1 in neonatal
53 OPC and for DNMT3A in adult OPC.

54

55

56 **Significance Statement**

57 The regenerative therapy of enhancing remyelination is the subject of much current
58 investigation for a number of central nervous system disorders. However, its mechanisms
59 remain incompletely understood. A recent study identified a distinct role of the DNA
60 methyltransferase 1 (DNMT1) in developmental myelination; here we report a dominant role for

eNeuro Accepted Manuscript

61 DNMT3A in adult remyelination after lysolecithin-induced demyelination. Overall this is of high
62 relevance as it indicates that neonatal and adult oligodendrocyte progenitor cells might be
63 characterized by distinct epigenetic landscapes that may need to be taken into consideration for
64 the development of future therapeutic strategies.
65
66
67 **Introduction**

68 In demyelinating disorders, such as multiple sclerosis (MS), loss of myelin sheaths
69 disturbs axonal conduction and trophic support, which eventually lead to irreversible axonal loss
70 and disease progression (Franklin et al., 2012; Nave and Trapp, 2008; Trapp et al., 1998).
71 Remyelination, which restores myelin sheaths to demyelinated axons and thereby restores both
72 axonal function and protection, is regarded as a promising way to prevent disease progression
73 (Dubois-Dalcq et al., 2008; Franklin and Ffrench-Constant, 2008). Oligodendrocyte progenitor
74 cells (OPC) have been identified as the main source for new myelin formation in the adult
75 central nervous system (CNS) (Zawadzka et al., 2010). Therefore, a better understanding of the
76 molecular mechanism regulating their differentiation into myelin-forming cells is highly desirable.
77 It has been proposed that after demyelination, adult OPC differentiation recapitulate
78 developmental myelination to a large extent, and the expression of well-established
79 differentiation regulatory transcription factors (e.g., *Myrf*, *Nkx2.2, Tcf4, Sox2*) has been shown to
80 change during remyelination (Fancy et al., 2004, 2009; Koenning et al., 2012; Moyon et al.,
81 2015; Zhao et al., 2015).

82 The importance of post-translational histone modifications during remyelination has
83 previously been reported (Shen et al., 2008). Recently, it has been shown that DNA methylation
84 mediated by the DNA methyltransferase DNMT1 is essential for developmental myelination,
85 where it controls the transition from the proliferative OPC stage to differentiating
86 oligodendrocytes (OL) (Moyon et al., 2016). In this study, we asked whether similar epigenetic

eNeuro Accepted Manuscript

87 mechanisms might be involved in the regulation of adult OPC differentiation during
88 remyelination. Transcriptomic data gathered from laser micro-dissected regions of CNS white
89 matter at various times following acute experimentally induced demyelination indicate that the
90 expression of *Dnmt1* and *Dnmt3a* are differentially regulated during remyelination (Huang et al.,
91 2011). Both enzyme levels were higher at 5dpl, during the early stages of remyelination and
92 lower at 14dpl and 28dpl, suggesting that DNA methylation might also play a role in the
93 transition from adult OPC to myelinating OL. A recent study has previously reported genome-
94 wide DNA methylation changes in post-mortem brain samples from MS patients compared to
95 controls, suggesting an underlying dysregulation of DNA methylation in MS brains (Huynh et al.,
96 2014).
97 This study directly addresses the role of DNA methylation in oligodendroglial lineage
98 cells during remyelination in the adult spinal cord. Here we show that DNA methylation and DNA
99 methyltransferases levels are differentially regulated during remyelination. We use lineage-
100 specific inducible genetic ablation of *Dnmt1* and/or *Dnmt3a* in adult mice to address the
101 functional relevance of DNA methylation perturbations for adult OPC differentiation and for the
102 efficiency of remyelination after experimentally-induced demyelination.
103
104
105 **Materials and Methods**
106 *Animals.* All experiments were performed according to IACUC-approved protocols and mice
107 were maintained in a temperature- and humidity-controlled facility on a 12-h light-dark cycle with
108 food and water *ad libitum*. *Dnmt1*$^{fl/fl}$ (Fan et al., 2001; Jackson-Grusby et al., 2001,
109 RRID:MMRRC_014114-UCD) and *Dnmt3a*$^{fl/fl}$ (Kaneda et al., 2004, RRID:MGI:3718448) mice
110 on a C57BL/6 background were crossed with *Plp-creER(t)* (Jackson Laboratory,
111 RRID:MGI:3696409) (Doerflinger et al., 2003).

eNeuro Accepted Manuscript

112 *Lysolecithin injections.* Injections were carried out in the ventrolateral spinal cord white matter of
113 8-week-old animals of either sex, as previously described (Fancy et al., 2009). Briefly,
114 anesthesia was induced and maintained with inhalational isoflurane/oxygen. The vertebral
115 column was fixed between metal bars on stereotaxic apparatus. The spinal vertebra was
116 exposed, tissue was cleared overlying the intervertebral space and the dura was pierced. A
117 pulled glass needle was advanced through the spine, at an angle of 70°, and 1μL of 1%
118 lysolecithin (Sigma L4129) was slowly injected into the ventrolateral white matter. Mice were
119 sutured and kept in a warm chamber during recovery.
120 *Tamoxifen injections.* 4-Hydroxytamoxifen (Sigma T56-48) was dissolved at 40mg/mL in 10%
121 ethanol and 90% corn oil (Sigma C8267) for 4 hours at 37ºC with rotation. 10mg was
122 administrated by gavage to each mouse at days 3, 5 and 7 (for 14dpl analysis) or at days 5, 7
123 and 9 (21dpl analysis) after LPC injection (day 0).
124 Immunohistochemistry. For immunohistochemistry, animals were perfused at 5 day-post-lesions
125 (dpl), 14dpl or 21dpl with 4% paraformaldehyde and post-fixed overnight in the same solution at
126 4°C. Spinal cords were dissected, cryo-protected in sucrose solutions and frozen embedded in
127 OCT. Immunohistochemistry was performed on 12μm cryostat sections. Antigen retrieval was
128 performed for 5-mC staining by incubating slides in sub-boiling (94°C) citrate buffer (pH 6.0) for
129 15 minutes. Slides were incubated in blocking buffer (5% normal donkey serum in PBS/Triton-
130 X100 0.3%) for 1 hour at room temperature and then overnight at 4°C with the primary
131 antibodies diluted in a similar blocking buffer (5% normal donkey serum in PBS/Triton-X100
132 0.3%). After rinsing with PBS 1X, sections were incubated with the Alexa Fluor secondary
133 antibodies and then washed with PBS 1X. Cell nuclei were counterstained with DNA fluorescent
134 dye Hoechst 33342 (Sigma B2261) in PBS. Stained tissue or cells were coverslipped in
135 FluorSave mounting medium (Millipore 345789) and examined on a Zeiss Axio Observer
136 Fluorescence Microscope. To quantify the data generated by immunohistochemical staining,

eNeuro Accepted Manuscript

137 counts were undertaken by an observer who was blinded to the experimental group from which
138 the sample being analysed was taken. Counts were made throughout the entire lesion area
139 which was scanned using the x20 objective of an AxioVision Observer A1 Zeiss flourescence
140 microscope. Labelled cells were manually counted from the images captured under the same
141 exposure conditions. AxioVision Rel4.8 software (RRID:SCR_002677) was used for co-localised
142 colour identification and area measurement. Quantification of total cell number, as defined by
143 nuclear (DAPI) staining, was assessed both within the lesion area and within the corresponding
144 region of white matter in unlesioned tissue.
145 To assess the levels of 5-mC in OLIG2+ cells, arbitrarily defined as being either low, medium or
146 high-5, a macro was created in ImageJ (RRID:SCR_003070) that first localised the OLIG2+(red)
147 nuclei and then measured the intensity of the 5mC (green) staining within the nuclear area. The
148 intensity value was then normalised by deducting the background staining intensity. For all
149 quantifications a minimum of 3 sections of 12 μm thickness from each lesion randomly chosen
150 from n = 4-6 mice was examined. The percentage or density of cells was determined per
151 mouse. The average and standard error was then calculated for each group using GraphPad
152 Prism Software (GraphPad Software, Inc, RRID:SCR_002798).
153 *Antibodies.* Primary antibodies used are: mouse anti-5-mC (Abcam, ab10805,
154 RRID:AB_442823, 1:200), mouse anti-CC1/APC (Millipore OP80, RRID:AB_2057371, 1:300),
155 rabbit anti-DNMT1 (Abcam, ab19905, RRID:AB_731983, 1:1,000), rabbit anti-DNMT3A (Santa
156 Cruz, sc-20703, RRID:AB_2093990, 1:500), mouse anti-NKX2.2 (Developmental Studies
157 Hybridoma Bank, University of Iowa, Iowa City, IA, 1:100), rabbit anti-OLIG2 (Millipore, ab9610,
158 RRID:AB_10141047, 1:1,000). Alexa Fluor conjugated secondary antibodies (1:5,000) were
159 used (Invitrogen).
160 *Electron microscopy.* For electron microscopy, animals were perfused at 21dpl with 4%
161 glutaraldehyde in PBS containing 0.4mM $CaCl_2$ and post-fixed in the same solution at 4°. The
162 spinal cord was coronally sliced at 1mm thickness and treated with 2% osmium tetroxide

eNeuro Accepted Manuscript

163 overnight before being subjected to a standard protocol for epoxy resin embedding (Zhao et al.,
164 2008) Tissues were sectioned at 1µm and stained with toluidine-blue. Remyelination ranking, in
165 which lesions with the greatest extent of remyelination were assigned the highest rank value,
166 was performed under light microscopy (Ito et al., 2007). Ultrathin sections of the lesion site were
167 cut onto copper grids and stained with uranyl acetate before being examined with a Hitachi H-
168 600 Transmission Electron Microscope. G-ratio was quantified on 50nm sections on a minimum
169 of 70 myelinated and remyelinated axons per animal, and 3 to 5 mice for each genotype.
170 *Statistical analysis.* All statistical analyses were done using GraphPad Prism (GraphPad
171 Software, Inc, RRID:SCR_002798). Unpaired student's t-test was used for every two datasets
172 with equal variances and for which data follow a normal distribution. If not normal,
173 nonparametric Mann Whitney test was used (for rankings analysis), and if the variances were
174 significantly different, the Welch's correction was applied (for g-ratio analysis). Two-way ANOVA
175 was used to compare three or more sets of data. For all graphs, error bars are mean±SEM.
176

	Data structure	Type of test	95% CI
[a] (Fig. 1C)	Normal distribution, equal variances	ANOVA and Bonferrroni posttests	108.6 to 272.7, -27.42 to 136.7 and -73.69 to 90.40
[b] (Fig. 1D)	Normal distribution, equal variances	ANOVA and Bonferrroni posttests	51.11 to 98.17 and 11.76 to 58.82 (5dpl); 33.78 to 80.84 and -11.49 to 35.57 (14dpl); 25.89 to 72.95 and -14.29 to 32.77 (21dpl)
[c] (Fig. 1F)	Normal distribution, equal variances	ANOVA and Bonferrroni posttests	45.42 to 116.2, 176.9 to 247.7 and 133.9 to 204.7
[d] (Fig. 1G)	Normal distribution,	ANOVA and	-2.914 to 37.65 and 60.67 to 101.2

eNeuro Accepted Manuscript

	equal variances	Bonferrroni posttests	(5dpl); -5.602 to 34.96 and 77.53 to 118.1 (14dpl); -13.63 to 26.93 and 53.74 to 94.30 (21dpl)
[e] (Fig.1I)	Normal distribution, equal variances	ANOVA and Bonferrroni posttests	-73.29 to -34.94, -70.07 to -31.72 and -85.01 to -46.66 (Low); 19.25 to 57.60, 8.444 to 46.79 and 16.22 to 54.56 (Medium); -4.294 to 34.05, 4.099 to 42.45, 11.27 to 49.62 (High)
[f] (Fig. 2B)	Normal distribution, equal variances	Student's t-test	201.1 to 231.7 (OLIG2+), 191.3 to 215.4 (CC1+)
[g] (Fig. 2D)	Normal distribution, equal variances	Student's t-test	210.2 to 205.7 (OLIG2+), 203.9 to 189.2 (CC1+)
[h] (Fig. 2F)	Normal distribution, equal variances	Student's t-test	178.2 to 144.9 (OLIG2+), 165.7 to 136.2 (CC1+)
[i] (Fig.2H)	Normal distribution, equal variances	ANOVA and Bonferrroni posttests	70.83 to 72.29 (Low); 15.67 to 13.36 (Medium); 13.50 to 14.35 (High)
[j] (Fig.2I)	Normal distribution, equal variances	ANOVA and Bonferrroni posttests	77.96 to 65.61 (Low); 15.85 to 23.22 (Medium); 6.186 to 11.17 (High)
[k] (Fig.2J)	Normal distribution, equal variances	ANOVA and Bonferrroni posttests	67.91 to 58.45 (Low); 21.32 to 31.39 (Medium); 10.77 to 10.16

			(High)
[l] (Fig. 3B)	Normal distribution, equal variances	Student's t-test	-307.8 to 246.4 (OLIG2+), -249.9 to 105.2 (CC1+) and -16.51 to 17.07 (CC1+/OLIG2+)
[m] (Fig. 3D)	Normal distribution, equal variances	Student's t-test	-341.1 to 431.1 (OLIG2+), 13.87 to 270.7 (CC1+) and 2.758 to 17.22 (CC1+/OLIG2+)
[n] (Fig. 3F)	Normal distribution, equal variances	Student's t-test	-275.5 to 52.4 (OLIG2+), 12.91 to 264.6 (CC1+) and 17.64 to 38.55 (CC1+/OLIG2+)
[o] (Fig. 3G)	Normal distribution, equal variances	Student's t-test	36.15 to 226.8 (DNMT1) and -136.3 to 15.88 (DNMT3A); -134.3 to -21.63 (DNMT1) and 48.69 to 246.2 (DNMT3A); 51.76 to 317.0 (DNMT1) and 106.9 to 307.9 (DNMT3A)
[p] (Fig.4B)	Normal distribution, equal variances	ANOVA and Bonferrroni posttests	22.94 to 25.45 (Low); 59.72 to 59.83 (Medium); 17.33 to 14.72 (High)
[q] (Fig.4D)	Normal distribution, equal variances	ANOVA and Bonferrroni posttests	22.71 to 31.26 (Low); 58.99 to 55.91 (Medium); 18.30 to 12.83 (High)
[r] (Fig.4F)	Normal distribution, equal variances	ANOVA and Bonferrroni posttests	21.26 to 37.88 (Low); 61.43 to 49.48 (Medium); 17.31 to 12.64 (High)

eNeuro Accepted Manuscript

eNeuro Accepted Manuscript

[s] (Fig. 5B)	Non-normal distribution	Nonparametric Mann Whitney test	2.648 to 11.35 and 1.362 to 7.838
[t] (Fig. 5C)	Normal distribution, unequal variances	Student's t-test with Welch's correction	-0.005297 to 0.005700
[u] (Fig. 5E)	Non-normal distribution	Nonparametric Mann Whitney test	1.823 to 11.38 and 2.191 to 9.142
[v] (Fig. 5F)	Normal distribution, unequal variances	Student's t-test with Welch's correction	-0.001182 to 0.01204
[x] (Fig. 5H)	Non-normal distribution	Nonparametric Mann Whitney test	-1.006 to 9.256 and 2.886 to 6.864
[y] (Fig. 5G)	Normal distribution, unequal variances	Student's t-test with Welch's correction	-0.01370 to -0.003870

Results

DNA methyltransferases are differently expressed in adult OPC during remyelination

To begin characterizing the role of DNA methylation in the oligodendroglial lineage during remyelination, we performed lysolecithin injections in the ventrolateral spinal cord of 8-week-old C57BL/6 mice and perfused them at 5-day-post-lesion (5dpl), 14dpl and 21dpl, to access DNA methyltransferases 1 and 3A (DNMT1 and DNMT3A) and 5-methylcytosine (5-mC) expression in oligodendrocyte progenitor cells (OPC) and oligodendrocytes (OL) (Fig. 1*A*). The number of NKX2.2+ oligodendroglial cells strongly expressing DNMT1, while abundant at 5 dpl when compared to levels in surrounding intact non-lesioned white matter (NWM), decreased between 5dpl and 21dpl (Fig. 1*B*-*C*). Co-staining of DNMT1 with CC1, a marker of mature OL,

eNeuro Accepted Manuscript

or NKX2.2, a marker of OPCs, revealed that within the CC1+ population the enzyme was expressed in 35.3±6.3% (5dpl), 12.0±5.4% (14dpl) and 9.2±5.6% (21dpl) of cells, while in the NKX2.2+ population, it was expressed in 74.6±5.3% (5dpl), 57.3±11.1% (14dpl) and 49.4±4.0% (21dpl) of cells (Fig. 1*B* and Fig. 1*D*). In contrast, the distribution of DNMT3A showed a different pattern, being strongly expressed by CC1+ cells and increased from 5dpl to 14pdl (Fig. 1*E*-*F*). Indeed, DNMT3A was expressed in 81.0±7.6% (5dpl), 97.8±1.9% (14dpl) and 74.0±9.3% (21dpl) of the CC1+ OL population and only in 17.4±3.8% (5dpl), 14.7±4.0% (14dpl) and 6.7±4.4% (21dpl) of the NKX2.2+ population (Fig. 1*E* and Fig. 1*G*). These data indicate distinct patterns of expression, with DNMT1 mainly expressed by adult OPC during the early stages of remyelination, and DNMT3A mainly detected in differentiated adult OL that appear in the later stages of remyelination.

We also quantified 5-mC expression levels in oligodendroglial cells. Because of species similarities in the 5-mC antibodies and those we had used for the OL lineage, we combined 5-mC staining with the pan-OL lineage marker OLIG2. This revealed a decreased proportion of low-methylated and increased proportion of medium- and high-methylated oligodendroglial cells during remyelination (Fig. 1*H*-*I*). Hyper-methylation in OLIG2+ cells was already evident starting 5dpl (Fig. 1*I*).

Ablation of DNMT3A and both DNMT1 and 3A impairs oligodendrocyte differentiation during remyelination

To address more specifically the functional role of DNA methylation in adult OPC during remyelination, we crossed the $Dnmt1^{fl/fl}$ and $Dnmt3a^{fl/fl}$ lines with the inducible *Plp-creER(t)*, to target specific ablation of *Dnmt1*, *Dnmt3a*, or both *Dnmt1* and *Dnmt3a* in PLP-expressing oligodendroglial cells after lysolecithin-induced demyelination. All three mutants ($Plp^{creER(t)/+}$:$Dnmt1^{fl/fl}$; $Plp^{creER(t)/+}$:$Dnmt3a^{fl/fl}$; and $Plp^{creER(t)/+}$:$Dnmt1^{fl/fl}$;$Dnmt3a^{fl/fl}$) and control littermates ($Plp^{+/+}$:$Dnmt1^{fl/fl}$; $Plp^{+/+}$:$Dnmt3a^{fl/fl}$ and $Plp^{+/+}$:$Dnmt1^{fl/fl}$;$Dnmt3a^{fl/fl}$) were gavaged with

eNeuro Accepted Manuscript

215 tamoxifen at 3dpl, 5dpl and 7dpl and then lesion-containing tissue harvested at 14dpl and
216 processed for immunohistochemistry using antibodies specific for 5-mC, for mature
217 oligodendrocytes (CC1) or for all cells within the oligodendrocyte lineage (OLIG2).

218 We first quantified the number of OLIG2 and CC1+ in NWM to address the effect of
219 *Dnmt1* and/or *Dnmt3a* ablation itself on the generation of OPCs and OLs (Fig. 2*A*-*F*). We
220 detected no difference in the number of OLIG2+ and CC1+ cells in any knock-out compared to
221 control NWM (Fig. 2*B*, 2*D*, 2*F*). Moreover, there was no differences in 5-mC expression levels in
222 OLIG2+ cells in knock-out compared to control NWM (Fig. 2*G*-*J*).

223 At 14dpl, there was no difference in the number of OLIG2+ and CC1+ cells in the lesion
224 or in the percentage of CC1+ differentiated OL among the OLIG2+ oligodendroglial cells
225 between *Plp*$^{+/+}$;*Dnmt1*$^{fl/fl}$ controls and *Plp*$^{creER(t)/+}$;*Dnmt1*$^{fl/fl}$ mutants (Fig. 3*A*-*B*). Ablation of
226 *Dnmt3a* resulted in a significant decrease of the percentage of CC1+ differentiated OL among
227 the OLIG2+ oligodendroglial cells (Fig. 3*C*-*D*). This indicated that OPC differentiation was
228 altered in mutants lacking *Dnmt3a*, while OLIG2+ proliferation and recruitment to the lesion was
229 not affected (Fig. 3D). It was noteworthy that increased DNMT1 levels were detected in CC1+
230 cells in *Plp*$^{creER(t)/+}$;*Dnmt3a*$^{fl/fl}$ mutant spinal cords, suggesting that in the absence of DNMT3A
231 there might be a compensatory increase in DNMT1 (Fig. 3*G*). To offset this possible effect, we
232 performed a similar analysis on double knock-out mice lacking both *Dnmt1* and *Dnmt3a*. Both
233 the number of CC1+ cells in the lesion and the percentage of CC1+ differentiated OL among the
234 OLIG2+ oligodendroglial cells were decreased in the double (*Plp*$^{creER(t)/+}$:*Dnmt1*$^{fl/fl}$;*Dnmt3a*$^{fl/fl}$)
235 mutants, and to a greater extent than we observed in the *Dnmt3a*-only ablated
236 (*Plp*$^{creER(t)/+}$;*Dnmt3a*$^{fl/fl}$) mutants (Fig. 3*E*-*F*).

237 There were no changes in 5-mC expression levels in OLIG2+ cells in *Plp*$^{creER(t)/+}$;*Dnmt1*$^{fl/fl}$
238 and *Plp*$^{creER(t)/+}$;*Dnmt3a*$^{fl/fl}$ mutants (Fig. 4*A*-*D*). However, there was an increase in the
239 percentage of low 5-mC expressing OLIG2+ cells, associated with a decrease of medium 5-mC
240 expressing OLIG2+ cells in the double *Plp*$^{creER(t)/+}$:*Dnmt1*$^{fl/fl}$;*Dnmt3a*$^{fl/fl}$ mutants (Fig. 4*E*-*F*). This

eNeuro Accepted Manuscript

241 suggested an increase in low-methylated and a decrease in medium-methylated
242 oligodendroglial cells in *Dnmt1/Dnmt3a* ablated mutants, which contrasted with the increased
243 methylation previously observed in control animals (Fig. 1*H-I*).
244 These data indicate a role for DNMT3A in adult OPC differentiation during remyelination
245 that can be compensated for by DNMT1.
246
247 **Ablation of *Dnmt1* and *Dnmt3a* impairs remyelination in the adult spinal cord**
248 To establish whether the impaired differentiation of OPC lacking DNMTs affected
249 remyelination we used a similar experimental design where we sacrificed lesioned control and
250 mutant mice at 21dpl, and evaluated remyelination by light microscopic examination of semi-thin
251 resin sections stained with toluidine blue and by electron microscopy. Comparison of control
252 and mutants NWM revealed no abnormalities in myelination in the three knock-out mice lines
253 (data not shown). Ranking of remyelination on semi-thin sections (Fig. 3*A-B* and Fig. 3*D-E*) and
254 quantification of the g-ratio (Fig. 3*C* and Fig. 3*F*) did not reveal any differences from controls for
255 either *Dnmt1*-ablated or *Dnmt3a*-ablated mice. In contrast, despite a similar ranking of
256 remyelination in sections from controls and double mutants (both *Dnmt1* and *Dnmt3a* ablated)
257 (Fig. 3*G-H* and Fig. 3*J*), the quantification of g-ratio revealed thinner myelin in mutants, likely
258 suggesting delayed remyelination in the absence of *Dnmt1* and *Dnmt3a* (Fig. 3*I*). This suggest
259 that if *Dnmt3a*-only ablation is sufficient to reduce adult OPC differentiation in an LPC-induced
260 lesion, compensation by DNMT1 might prevent significantly delayed remyelination.
261 These data demonstrate that dysregulation of DNA methylation in adult oligodendroglial
262 cells impairs their differentiation and hence their ability to contribute to remyelination.
263
264
265 **Discussion**

eNeuro Accepted Manuscript

266 Here we report that DNMT1 and DNMT3A are differentially expressed during
267 remyelination after lysolecithin-induced demyelination in the adult spinal cord, with DNMT1
268 being highly expressed in OPC at early time points after demyelination (corresponding in this
269 model to the early stages of remyelination) and DNMT3A being highly expressed in OL at later
270 time points (corresponding to the later stages and completion of remyelination). These data
271 validate and extend previous microarray-generated data obtained in laser-capture
272 microdissected tissues from rats with ethidium bromide-induced demyelinating lesions, which
273 revealed initial increased expression of both *Dnmt1* and *Dnmt3a* and their subsequent decrease
274 in expression (Huang et al., 2011). Discordance between the two studies, especially for
275 DNMT3A expression, can be explained by differences in the experimental approach. The Huang
276 et al. dataset was obtained from whole tissue, which has a mixed composition and percentage
277 of various cell types at different time points, possibly impacting the levels of transcripts. Indeed,
278 *Dnmt1* and *Dnmt3a* are also highly expressed by astrocytes and microglial cells, the latter being
279 massively abundant in the lesion at 5dpl but less abundant during the later stages (Zhang et al.,
280 2014).

281 Our study reports global hypermethylation in the nuclei of oligodendroglial lineage cells
282 during remyelination, similar to what described during developmental myelination (Moyon et al.,
283 2016). These data suggested that adult OPC differentiation might recapitulate their
284 developmental differentiation, by activating same transcriptional pathways and perhaps the
285 same epigenetic modulators (Fancy et al., 2004, 2009; Koenning et al., 2012; Moyon et al.,
286 2015; Nakatani et al., 2013; Zhao et al., 2015). Indeed, chromatin remodelers (*i.e. Chd7* and
287 *Brg1*) and histone deacetylases have been recently shown to be essential for OPC myelination
288 as well as remyelination (He et al., 2016; Shen et al., 2008).

289 Using conditional knock-out murine strains, we showed that lack of *Dnmt3a*, and not
290 *Dnmt1*, in oligodendroglial cells impairs adult OPC differentiation. These data differed from the
291 findings obtained during development, where the ablation of *Dnmt1*, and not *Dnmt3a*, resulted in

eNeuro Accepted Manuscript

292 extensive defective myelination of the CNS (Moyon et al., 2016). We also observed that,
293 contrary to developmental data, loss of *Dnmt3a* was partially compensated by upregulation of
294 *Dnmt1* levels, leading to decreased adult OPC differentiation and remyelination delays in the
295 double conditional knock-out mice. It is important to highlight that the *Plp-creER(t)* line was used
296 to target oligodendroglial lineage in an inducible manner in the adult spinal cord. Although PLP
297 has been shown to be expressed in adult OPC (Lin et al., 2009; Ruffini et al., 2004; Spassky et
298 al., 1998), our ablation of *Dnmt1* and *Dnmt3a* may have targeted a more mature population,
299 when cells have already exited cell cycle and thus, when DNMT1 and DNMT3A might have a
300 different impact. The remyelination delay observed here is also less drastic than the extensive
301 and global hypomyelination affecting the $Olig1^{cre/+}$;$Dnmt1^{fl/fl}$ mutant mice (Moyon et al., 2016).
302 Adult OPC tend to proliferate less than their neonatal counterparts, suggesting that the absence
303 of DNMT1 may not as adversely affect their replication, cell division and survival (Lin et al.,
304 2009; Moyon et al., 2015; Ruffini et al., 2004; Shi et al., 1998; Wolswijk and Noble, 1989;
305 Wolswijk et al., 1991; Young et al., 2013). Moreover, some epigenetic marks might have been
306 already established and could be irreversibly maintained in adult OPC, which are emerging from
307 a pool of undifferentiating neonatal OPC (Zawadzka et al., 2010). Indeed, it has been shown
308 that in cell lines epigenetic marks such as histone methylation, histone deacetylation and DNA
309 methylation might have specific dynamics, with some being partial committers and others
310 complete committers, depending of their enzyme recruitment speed and affinity at specific
311 genomic sites (Bintu et al., 2016). For example, the *de novo* embryonic DNMT3B is a slow
312 silencer but complete committer, as its methylated marks could not be easily removed. Thus, it
313 could explain why ablation of *Dnmt3a* in adult OPC might have a limited affect and only delays
314 remyelination, as its marks would be maintained long after the enzyme ablation.

315 Finally, DNA methylation has been shown to be dysregulated in several neurological
316 pathologies, including amyotrophic lateral sclerosis, schizophrenia and oligodendroglial
317 pathologies such as MS and gliomas (Chou et al., 2012; Hannon et al., 2016; Huynh et al.,

eNeuro Accepted Manuscript

318 2014; Jaffe et al., 2016; Martin and Wong, 2013). In addition to neuropathy, dementia and
319 hearing loss, patients with DNA methyltransferases (*DNMT1*) mutations present with mild CNS
320 hypomyelination (Klein et al., 2011). Epigenome-wide methylation study has identified several
321 hypermethylated or hypomethylated loci in MS patients post-mortem brain tissues compared to
322 controls (Huynh et al., 2014) and several studies in gliomas have described an extensive global
323 DNA hypomethylation (Chou et al., 2012; Watanabe and Maekawa, 2010) associated with site-
324 specific DNA hypermethylation (Felsberg et al., 2006; Sharma et al., 2010). Further epigenome-
325 wide studies should be performed on adult OPC to specifically identify genomic loci that might
326 be hypo- or hyper-methylated during their proliferation and their differentiation, in control
327 conditions and after demyelination or in gliomas. We propose that modulating DNA methylation
328 in oligodendroglial cells could efficiently regulate adult OPC proliferation and differentiation
329 capacities. Targeting DNA methylation at specific genomic loci, using engineered zinc fingers or
330 CRISPR-Cas9 methylation modulators, might lead to the development of new therapeutic
331 strategies in gliomas and MS (Choudhury et al., 2014; Heller et al., 2014; McDonald et al.,
332 2016).

333

334

335 **References**

336 Bintu, L., Yong, J., Antebi, Y.E., McCue, K., Kazuki, Y., Uno, N., Oshimura, M., and Elowitz,
337 M.B. (2016). Dynamics of epigenetic regulation at the single-cell level. Science *351*, 720–724.

338 Chou, A.P., Chowdhury, R., Li, S., Chen, W., Kim, A.J., Piccioni, D.E., Selfridge, J.M., Mody,
339 R.R., Chang, S., Lalezari, S., et al. (2012). Identification of Retinol Binding Protein 1 Promoter
340 Hypermethylation in Isocitrate Dehydrogenase 1 and 2 Mutant Gliomas. J. Natl. Cancer Inst.
341 *104*, 1458–1469.

eNeuro Accepted Manuscript

342 Choudhury, S.R., Cui, Y., Lubecka, K., Stefanska, B., and Irudayaraj, J. (2014). CRISPR-dCas9
343 mediated TET1 targeting for selective DNA demethylation at BRCA1 promoter. Oncotarget.

344 Doerflinger, N.H., Macklin, W.B., and Popko, B. (2003). Inducible site-specific recombination in
345 myelinating cells. Genes. N. Y. N 2000 *35*, 63–72.

346 Dubois-Dalcq, M., Williams, A., Stadelmann, C., Stankoff, B., Zalc, B., and Lubetzki, C. (2008).
347 From fish to man: understanding endogenous remyelination in central nervous system
348 demyelinating diseases. Brain *131*, 1686–1700.

349 Fan, G., Beard, C., Chen, R.Z., Csankovszki, G., Sun, Y., Siniaia, M., Biniszkiewicz, D., Bates,
350 B., Lee, P.P., Kuhn, R., et al. (2001). DNA hypomethylation perturbs the function and survival of
351 CNS neurons in postnatal animals. J Neurosci *21*, 788–797.

352 Fancy, S.P.J., Zhao, C., and Franklin, R.J. (2004). Increased expression of Nkx2.2 and Olig2
353 identifies reactive oligodendrocyte progenitor cells responding to demyelination in the adult
354 CNS. Mol Cell Neurosci *27*, 247–254.

355 Fancy, S.P., Baranzini, S.E., Zhao, C., Yuk, D.I., Irvine, K.A., Kaing, S., Sanai, N., Franklin,
356 R.J.M., and Rowitch, D.H. (2009). Dysregulation of the Wnt pathway inhibits timely myelination
357 and remyelination in the mammalian CNS. Genes Dev *23*, 1571–1585.

358 Felsberg, J., Yan, P.S., Huang, T.H.-M., Milde, U., Schramm, J., Wiestler, O.D., Reifenberger,
359 G., Pietsch, T., and Waha, A. (2006). DNA methylation and allelic losses on chromosome arm
360 14q in oligodendroglial tumours. Neuropathol. Appl. Neurobiol. *32*, 517–524.

361 Franklin, R.J.M., and Ffrench-Constant, C. (2008). Remyelination in the CNS: from biology to
362 therapy. Nat Rev Neurosci *9*, 839–855.

eNeuro Accepted Manuscript

363 Franklin, R.J.M., ffrench-Constant, C., Edgar, J.M., and Smith, K.J. (2012). Neuroprotection and
364 repair in multiple sclerosis. Nat Rev Neurol *8*, 624–634.

365 Hannon, E., Spiers, H., Viana, J., Pidsley, R., Burrage, J., Murphy, T.M., Troakes, C., Turecki,
366 G., O'Donovan, M.C., Schalkwyk, L.C., et al. (2016). Methylation quantitative trait loci in the
367 developing brain and their enrichment in schizophrenia-associated genomic regions. Nat.
368 Neurosci. *19*, 48–54.

369 He, D., Marie, C., Zhao, C., Kim, B., Wang, J., Deng, Y., Clavairoly, A., Frah, M., Wang, H., He,
370 X., et al. (2016). Chd7 cooperates with Sox10 and regulates the onset of CNS myelination and
371 remyelination. Nat. Neurosci. *19*, 678–689.

372 Heller, E.A., Cates, H.M., Peña, C.J., Sun, H., Shao, N., Feng, J., Golden, S.A., Herman, J.P.,
373 Walsh, J.J., Mazei-Robison, M., et al. (2014). Locus-specific epigenetic remodeling controls
374 addiction- and depression-related behaviors. Nat. Neurosci. *17*, 1720–1727.

375 Huang, J.K., Jarjour, A.A., Nait Oumesmar, B., Kerninon, C., Williams, A., Krezel, W.,
376 Kagechika, H., Bauer, J., Zhao, C., Evercooren, A.B., et al. (2011). Retinoid X receptor gamma
377 signaling accelerates CNS remyelination. Nat Neurosci *14*, 45–53.

378 Huynh, J.L., Garg, P., Thin, T.H., Yoo, S., Dutta, R., Trapp, B.D., Haroutunian, V., Zhu, J.,
379 Donovan, M.J., Sharp, A.J., et al. (2014). Epigenome-wide differences in pathology-free regions
380 of multiple sclerosis-affected brains. Nat. Neurosci. *17*, 121–130.

381 Ito, D., Fujita, N., Ibanez, C., Sasaki, N., Franklin, R.J.M., and Jeffery, N.D. (2007). Serum-Free
382 Medium Provides a Clinically Relevant Method to Increase Olfactory Ensheathing Cell Numbers
383 in Olfactory Mucosa Cell Culture. Cell Transplant. *16*, 1021–1027.

eNeuro Accepted Manuscript

384 Jackson-Grusby, L., Beard, C., Possemato, R., Tudor, M., Fambrough, D., Csankovszki, G.,
385 Dausman, J., Lee, P., Wilson, C., Lander, E., et al. (2001). Loss of genomic methylation causes
386 p53-dependent apoptosis and epigenetic deregulation. Nat. Genet. *27*, 31–39.

387 Jaffe, A.E., Gao, Y., Deep-Soboslay, A., Tao, R., Hyde, T.M., Weinberger, D.R., and Kleinman,
388 J.E. (2016). Mapping DNA methylation across development, genotype and schizophrenia in the
389 human frontal cortex. Nat. Neurosci. *19*, 40–47.

390 Kaneda, M., Okano, M., Hata, K., Sado, T., Tsujimoto, N., Li, E., and Sasaki, H. (2004).
391 Essential role for de novo DNA methyltransferase Dnmt3a in paternal and maternal imprinting.
392 Nature *429*, 900–903.

393 Klein, C.J., Botuyan, M.-V., Wu, Y., Ward, C.J., Nicholson, G.A., Hammans, S., Hojo, K.,
394 Yamanishi, H., Karpf, A.R., Wallace, D.C., et al. (2011). Mutations in DNMT1 cause hereditary
395 sensory neuropathy with dementia and hearing loss. Nat. Genet. *43*, 595–600.

396 Koenning, M., Jackson, S., Hay, C.M., Faux, C., Kilpatrick, T.J., Willingham, M., and Emery, B.
397 (2012). Myelin gene regulatory factor is required for maintenance of myelin and mature
398 oligodendrocyte identity in the adult CNS. J Neurosci *32*, 12528–12542.

399 Lin, G., Mela, A., Guilfoyle, E., and Goldman, J. (2009). Neonatal and adult O4(+)
400 oligodendrocyte lineage cells display different growth factor responses and different gene
401 expression patterns. J Neurosci Res *87*, 3390–3402.

402 Martin, L.J., and Wong, M. (2013). Aberrant regulation of DNA methylation in amyotrophic
403 lateral sclerosis: a new target of disease mechanisms. Neurother. J. Am. Soc. Exp. Neurother.
404 *10*, 722–733.

eNeuro Accepted Manuscript

405 McDonald, J.I., Celik, H., Rois, L.E., Fishberger, G., Fowler, T., Rees, R., Kramer, A., Martens,
406 A., Edwards, J.R., and Challen, G.A. (2016). Reprogrammable CRISPR/Cas9-based system for
407 inducing site-specific DNA methylation. Biol. Open.

408 Moyon, S., Dubessy, A.L., Aigrot, M.S., Trotter, M., Huang, J.K., Dauphinot, L., Potier, M.C.,
409 Kerninon, C., Parsadaniantz, S.M., Franklin, R.J.M., et al. (2015). Demyelination causes adult
410 CNS progenitors to revert to an immature state and express immune cues that support their
411 migration. J. Neurosci. *35*, 4–20.

412 Moyon, S., Huynh, J.L., Dutta, D., Zhang, F., Ma, D., Yoo, S., Lawrence, R., Wegner, M., John,
413 G.R., Emery, B., et al. (2016). Functional Characterization of DNA Methylation in the
414 Oligodendrocyte Lineage. Cell Rep. *15*, 748–760.

415 Nakatani, H., Martin, E., Hassani, H., Clavairoly, A., Maire, C.L., Viadieu, A., Kerninon, C.,
416 Delmasure, A., Frah, M., Weber, M., et al. (2013). Ascl1/Mash1 Promotes Brain
417 Oligodendrogenesis during Myelination and Remyelination. J Neurosci *33*, 9752–9768.

418 Nave, K.A., and Trapp, B.D. (2008). Axon-glial signaling and the glial support of axon function.
419 Annu Rev Neurosci *31*, 535–561.

420 Ruffini, F., Arbour, N., Blain, M., Olivier, A., and Antel, J.P. (2004). Distinctive properties of
421 human adult brain-derived myelin progenitor cells. Am J Pathol *165*, 2167–2175.

422 Sharma, S., Kelly, T.K., and Jones, P.A. (2010). Epigenetics in cancer. Carcinogenesis *31*, 27–
423 36.

424 Shen, S., Sandoval, J., Swiss, V., Li, J., Dupree, J., Franklin, R.J.M., and Casaccia-Bonnefil, P.
425 (2008). Age-dependent epigenetic control of differentiation inhibitors is critical for remyelination
426 efficiency. Nat Neurosci *11*, 1024–1034.

eNeuro Accepted Manuscript

427 Shi, J., Marinovich, A., and Barres, B.A. (1998). Purification and characterization of adult
428 oligodendrocyte precursor cells from the rat optic nerve. J Neurosci *18*, 4627–4636.

429 Spassky, N., Goujet-Zalc, C., Parmantier, E., Olivier, C., Martinez, S., Ivanova, A., Ikenaka, K.,
430 Macklin, W., Cerruti, I., Zalc, B., et al. (1998). Multiple restricted origin of oligodendrocytes. J
431 Neurosci *18*, 8331–8343.

432 Trapp, B.D., Peterson, J., Ransohoff, R.M., Rudick, R., Mörk, S., and Bö, L. (1998). Axonal
433 transection in the lesions of multiple sclerosis. N Engl J Med *338*, 278–285.

434 Watanabe, Y., and Maekawa, M. (2010). Methylation of DNA in cancer. Adv. Clin. Chem. *52*,
435 145–167.

436 Wolswijk, G., and Noble, M. (1989). Identification of an adult-specific glial progenitor cell.
437 Development *105*, 387–400.

438 Wolswijk, G., Riddle, P.N., and Noble, M. (1991). Platelet-derived growth factor is mitogenic for
439 O-2Aadult progenitor cells. Glia *4*, 495–503.

440 Young, K.M., Psachoulia, K., Tripathi, R.B., Dunn, S.J., Cossell, L., Attwell, D., Tohyama, K.,
441 and Richardson, W.D. (2013). Oligodendrocyte dynamics in the healthy adult CNS: evidence for
442 myelin remodeling. Neuron *77*, 873–885.

443 Zawadzka, M., Rivers, L.E., Fancy, S.P., Zhao, C., Tripathi, R., Jamen, F., Young, K.,
444 Goncharevich, A., Pohl, H., Rizzi, M., et al. (2010). CNS-resident glial progenitor/stem cells
445 produce Schwann cells as well as oligodendrocytes during repair of CNS demyelination. Cell
446 Stem Cell *6*, 578–590.

447 Zhang, Y., Chen, K., Sloan, S.A., Bennett, M.L., Scholze, A.R., O'Keeffe, S., Phatnani, H.P.,
448 Guarnieri, P., Caneda, C., Ruderisch, N., et al. (2014). An RNA-sequencing transcriptome and

eNeuro Accepted Manuscript

449 splicing database of glia, neurons, and vascular cells of the cerebral cortex. J. Neurosci. Off. J.
450 Soc. Neurosci. *34*, 11929–11947.

451 Zhao, C., Fancy, S.P.J., ffrench-Constant, C., and Franklin, R.J.M. (2008). Osteopontin is
452 extensively expressed by macrophages following CNS demyelination but has a redundant role
453 in remyelination. Neurobiol. Dis. *31*, 209–217.

454 Zhao, C., Ma, D., Zawadzka, M., Fancy, S.P.J., Elis-Williams, L., Bouvier, G., Stockley, J.H.,
455 Castro, G.M. de, Wang, B., Jacobs, S., et al. (2015). Sox2 Sustains Recruitment of
456 Oligodendrocyte Progenitor Cells following CNS Demyelination and Primes Them for
457 Differentiation during Remyelination. J. Neurosci. *35*, 11482–11499.

458

459

460 **Legends**

461 **Figure 1.** DNA methyltransferases are differently expressed in adult OPC during remyelination.
462 ***A*** Schematic of the lysolecithin-induced focal demyelination and of the area of NWM used for
463 quntification. ***B*** Representative DNMT1, NKX2.2 and CC1 stainings in normal white matter
464 (NWM) and at 5, 14 and 21dpl (white arrow heads indicate double-positive cells). ***C***
465 Quantification of the number of double DNMT1+ and NKX2.2+ cells at 5, 14 and 21dpl,
466 compared to NWM[a]. ***D*** Quantification of the percentage of double DNMT1+ and NKX2.2+ or
467 CC1+ cells at 5, 14 and 21dpl, compared to NWM[b]. ***E*** Representative DNMT3A, NKX2.2 and
468 CC1 stainings in NWM and at 5, 14 and 21dpl (white arrow heads indicate double-positive
469 cells). ***F*** Quantification of the number of double DNMT3A+ and CC1+ cells at 5, 14 and 21dpl,
470 compared to NWM[c]. ***G*** Quantification of the percentage of double DNMT3A+ and NKX2.2+ or
471 CC1+ cells at 5, 14 and 21dpl, compared to NWM[d]. ***H*** Representative 5-mC and OLIG2 staining
472 in NWM and at 5, 14 and 21dpl (white arrow heads indicate high-5mC+/OLIG2+ cells).

eNeuro Accepted Manuscript

473 Representative low-, medium- and high-5-mC cells are shown below. ***I*** Quantification of low-,
474 medium- and high-5-mC levels in OLIG2+ cells at 5, 14 and 21dpl, compared to NWM[e]. Scale
475 bar = 20 µm. Data are mean ± SEM. n=4-6 animals, 3 sections per animal. **p* < 0.05, ***p* < 0.01,
476 ****p* < 0.001 (ANOVA).

477 **Figure 2.** Ablation of *Dnmt1* and/or *Dnmt3a* does not impair oligodendrocyte differentiation or
478 their methylation levels in control conditions. ***A*** Representative OLIG2 and CC1 staining in
479 tamoxifen-treated $Plp^{+/+}$;$Dnmt1^{fl/fl}$ and $Plp^{creER(t)/+}$;$Dnmt1^{fl/fl}$ NWM spinal cords. ***B*** Quantification of
480 OLIG2+ and CC1+ cell densities in NWM[f] (p = 0.3537, p = 0.3803). ***C*** Representative OLIG2
481 and CC1 staining in tamoxifen-treated $Plp^{+/+}$;$Dnmt3a^{fl/fl}$ and $Plp^{creER(t)/+}$;$Dnmt3a^{fl/fl}$ NWM spinal
482 cords. ***D*** Quantification of OLIG2+ and CC1+ cell densities in NWM[g] (p = 0.8926, p = 0.5109). ***E***
483 Representative OLIG2 and CC1 staining in tamoxifen-treated $Plp^{+/+}$;$Dnmt1^{fl/fl}$;$Dnmt3a^{fl/fl}$ and
484 $Plp^{creER(t)/+}$;$Dnmt1^{fl/fl}$;$Dnmt3a^{fl/fl}$ NWM spinal cords. ***F*** Quantification of OLIG2+ and CC1+ cell
485 densities in NWM[h] (p = 0.3136, p = 0.2173). ***G*** Representative 5-mC and OLIG2 stainings in
486 tamoxifen-treated $Plp^{creER(t)/+}$;$Dnmt1^{fl/fl}$, $Plp^{creER(t)/+}$;$Dnmt3a^{fl/fl}$ and $Plp^{creER(t)/+}$;$Dnmt1^{fl/fl}$;$Dnmt3a^{fl/fl}$
487 NWM spinal cords (white arrow heads indicate high-5mC+/OLIG2+ cells). ***H*** Quantification of
488 low-, medium- and high-5-mC levels in OLIG2+ cells in tamoxifen-treated $Plp^{+/+}$;$Dnmt1^{fl/fl}$ and
489 $Plp^{creER(t)/+}$;$Dnmt1^{fl/fl}$ NWM[j]**.** ***I*** Quantification of low-, medium- and high-5-mC levels in OLIG2+
490 cells in tamoxifen-treated $Plp^{+/+}$;$Dnmt3a^{fl/fl}$ and $Plp^{creER(t)/+}$;$Dnmt3a^{fl/fl}$ NWM[jj]**.** ***J*** Quantification of
491 low-, medium- and high-5-mC levels in OLIG2+ cells in tamoxifen-treated
492 $Plp^{+/+}$;$Dnmt1^{fl/fl}$;$Dnmt3a^{fl/fl}$ and $Plp^{creER(t)/+}$;$Dnmt1^{fl/fl}$;$Dnmt3a^{fl/fl}$ NWM[k]**.** Scale bar = 50 µm. Data are
493 mean ± SEM. n=4-6 animals, 3 sections per animal. (Student's t-test, ANOVA).

494 **Figure 3.** Ablation of *Dnmt3a* and both *Dnmt1* and *Dnmt3a* impairs oligodendrocyte
495 differentiation during remyelination. ***A*** Representative OLIG2 and CC1 staining at 14dpl in
496 tamoxifen-treated $Plp^{+/+}$;$Dnmt1^{fl/fl}$ and $Plp^{creER(t)/+}$;$Dnmt1^{fl/fl}$ spinal cords. ***B*** Quantification of
497 OLIG2+ and CC1+ cell densities and CC1+ / OLIG2+ cells percentage at 14dpl[l] (p = 0.7955, p =

eNeuro Accepted Manuscript

498 0.3573, p = 0.9689). ***C*** Representative OLIG2 and CC1 staining at 14dpl in tamoxifen-treated
499 *Plp*$^{+/+}$;*Dnmt3a*$^{fl/fl}$ and *Plp*$^{creER(t)/+}$;*Dnmt3a*$^{fl/fl}$ spinal cords. ***D*** Quantification of OLIG2+ and CC1+
500 cell densities and CC1+ / OLIG2+ cells percentage at 14dpl[m] (p = 0.7851, p = 0.0550, p =
501 0.0149). ***E*** Representative OLIG2 and CC1 staining at 14dpl in tamoxifen-treated
502 *Plp*$^{+/+}$;*Dnmt1*$^{fl/fl}$;*Dnmt3a*$^{fl/fl}$ and *Plp*$^{creER(t)/+}$;*Dnmt1*$^{fl/fl}$;*Dnmt3a*$^{fl/fl}$ spinal cords. ***F*** Quantification of
503 OLIG2+ and CC1+ cell densities and CC1+ / OLIG2+ cells percentage at 14dpl[n] (p = 0.1510, p =
504 0.0357, p = 0.0006). ***G*** Quantification of DNMT1 and DNMT3A expression in CC1+ cells at
505 14dpl in tamoxifen-treated *Plp*$^{+/+}$;*Dnmt1*$^{fl/fl}$ and *Plp*$^{creER(t)/+}$;*Dnmt1*$^{fl/fl}$, *Plp*$^{+/+}$;*Dnmt3a*$^{fl/fl}$ and
506 *Plp*$^{creER(t)/+}$;*Dnmt3a*$^{fl/fl}$, *Plp*$^{+/+}$;*Dnmt1*$^{fl/fl}$;*Dnmt3a*$^{fl/fl}$ and *Plp*$^{creER(t)/+}$;*Dnmt1*$^{fl/fl}$;*Dnmt3a*$^{fl/fl}$ spinal cords,
507 to detect eventual compensation between DNMTs at the protein level[o] (p = 0.0075, p = 0.0505,
508 p = 0.0074, p = 0.0053, p = 0.0072, p = 0.0012). Scale bar = 20 µm. Data are mean ± SEM.
509 n=4-6 animals, 3 sections per animal. *p < 0.05, **p < 0.01, ***p < 0.001 (Student's t-test).

510 **Figure 4**. Ablation of *Dnmt3a* and both *Dnmt1* and *Dnmt3a* impairs methylation levels in
511 oligodendroglial cells during remyelination. ***A*** Representative 5-mC and OLIG2 staining at 14dpl
512 in tamoxifen-treated *Plp*$^{+/+}$;*Dnmt1*$^{fl/fl}$ and *Plp*$^{creER(t)/+}$;*Dnmt1*$^{fl/fl}$ spinal cords (white arrow heads
513 indicate high-5mC+/OLIG2+ cells). ***B*** Quantification of low-, medium- and high-5-mC levels in
514 OLIG2+ cells at 14dpl[p]. ***C*** Representative 5-mC and OLIG2 staining at 14dpl in tamoxifen-
515 treated *Plp*$^{+/+}$;*Dnmt1*$^{fl/fl}$ and *Plp*$^{creER(t)/+}$;*Dnmt3a*$^{fl/fl}$ spinal cords (white arrow heads indicate high-
516 5mC+/OLIG2+ cells). ***D*** Quantification of low-, medium- and high-5-mC levels in OLIG2+ cells at
517 14dpl[q]. ***E*** Representative 5-mC and OLIG2 staining at 14dpl in tamoxifen-treated *Plp*$^{+/+}$;*Dnmt1*$^{fl/fl}$
518 and *Plp*$^{creER(t)/+}$;*Dnmt1*$^{fl/fl}$;*Dnmt3a*$^{fl/fl}$ spinal cords (white arrow heads indicate high-5-mC+/OLIG2+
519 cells). ***F*** Quantification of low-, medium- and high-5-mC levels in OLIG2+ cells at 14dpl[r]. Scale
520 bar = 100 µm. Data are mean ± SEM. n=4-6 animals, 3 sections per animal. **p < 0.01, ***p <
521 0.001 (ANOVA).

eNeuro Accepted Manuscript

522 **Figure 5.** Ablation of *Dnmt1* and *Dnmt3a* impairs remyelination in the adult spinal cord. ***A***
523 Representative semi-thin sections at 21dpl in tamoxifen-treated $Plp^{+/+}$;$Dnmt1^{fl/fl}$ and
524 $Plp^{creER(t)/+}$;$Dnmt1^{fl/fl}$ spinal cords. ***B*** Relative ranking of remyelination[s] (p = 0.3075). ***C***
525 Quantification of G-ratios for control and mutants mice, and plot of G-ratios against axonal
526 diameter[t] (p = 0.9426). ***D*** Representative semi-thin sections at 21dpl in tamoxifen-treated
527 $Plp^{+/+}$;$Dnmt3a^{fl/fl}$ and $Plp^{creER(t)/+}$;$Dnmt3a^{fl/fl}$ spinal cords. ***E*** Relative ranking of remyelination[u] (p =
528 0.7144). ***F*** Quantification of G-ratios for control and mutants mice, and plot of G-ratios against
529 axonal diameter[v] (p = 0.1079). ***G*** Representative semi-thin sections at 21dpl in tamoxifen-
530 treated $Plp^{+/+}$;$Dnmt1^{fl/fl}$;$Dnmt3a^{fl/fl}$ and $Plp^{creER(t)/+}$;$Dnmt1^{fl/fl}$;$Dnmt3a^{fl/fl}$ spinal cords. ***H*** Relative
531 ranking of remyelination[x] (p = 0.7584). ***I*** Quantification of G-ratios for control and mutants mice,
532 and plot of G-ratios against axonal diameter[y] (p = 0.0005). ***J*** Representative electron
533 microscopic sections at 21dpl in tamoxifen-treated $Plp^{+/+}$;$Dnmt1^{fl/fl}$;$Dnmt3a^{fl/fl}$ and
534 $Plp^{creER(t)/+}$;$Dnmt1^{fl/fl}$;$Dnmt3a^{fl/fl}$ spinal cords revealing new thin myelin sheaths of remyelination
535 (arrows) and a demyelinated axon (arrow head). Scale bar = 10 µm. Dots are ranking for each
536 mouse (***B***, ***E***, ***H***) and G-ratio for each quantified axons (***C***, ***F***, ***I***). Data are mean ± SEM. n=3-5
537 animals, > 70 axons per animal. ***$p < 0.01$ (Mann Whitney test and Student's t-test).

538

eNeuro Accepted Manuscript

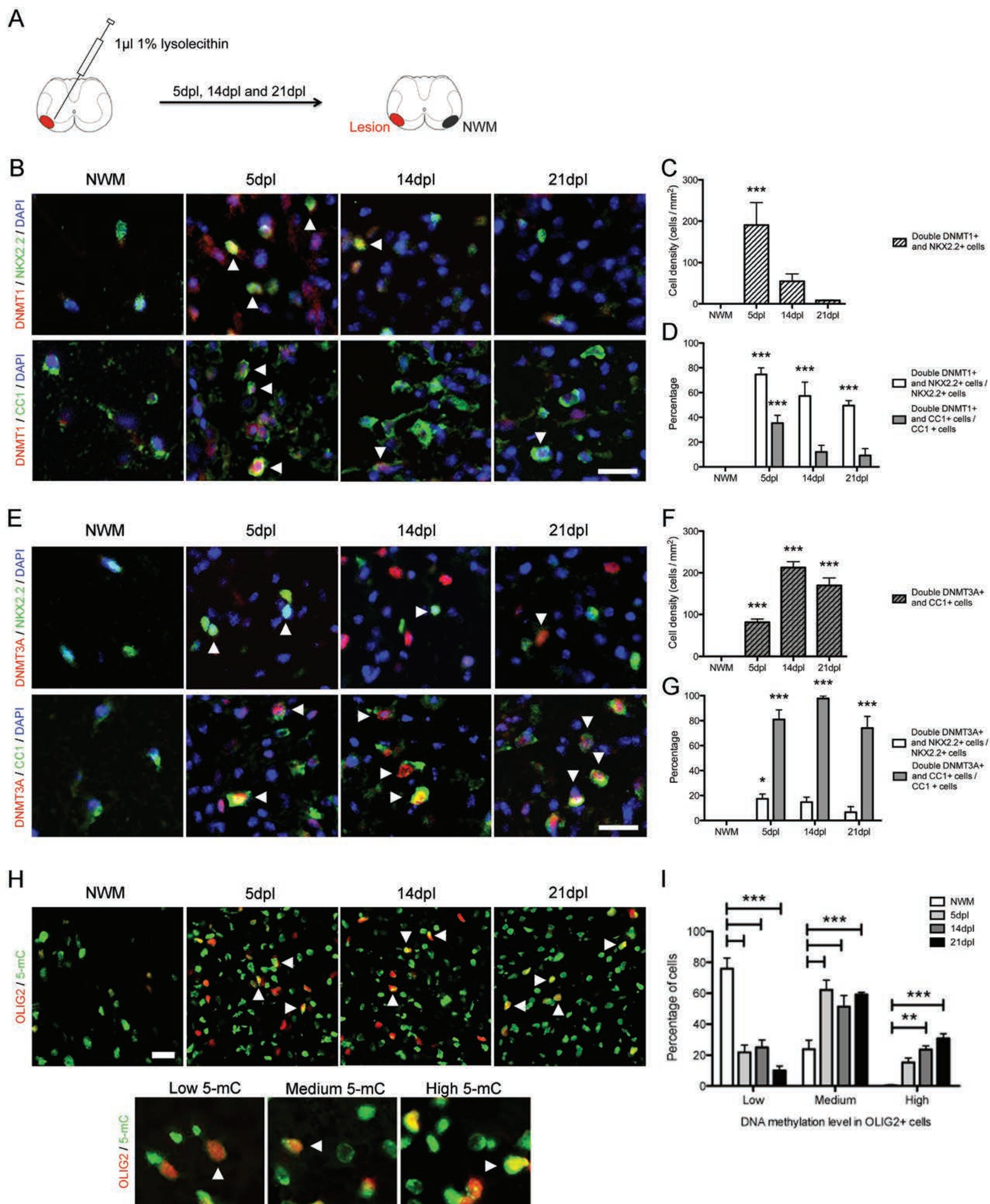

eNeuro Accepted Manuscript

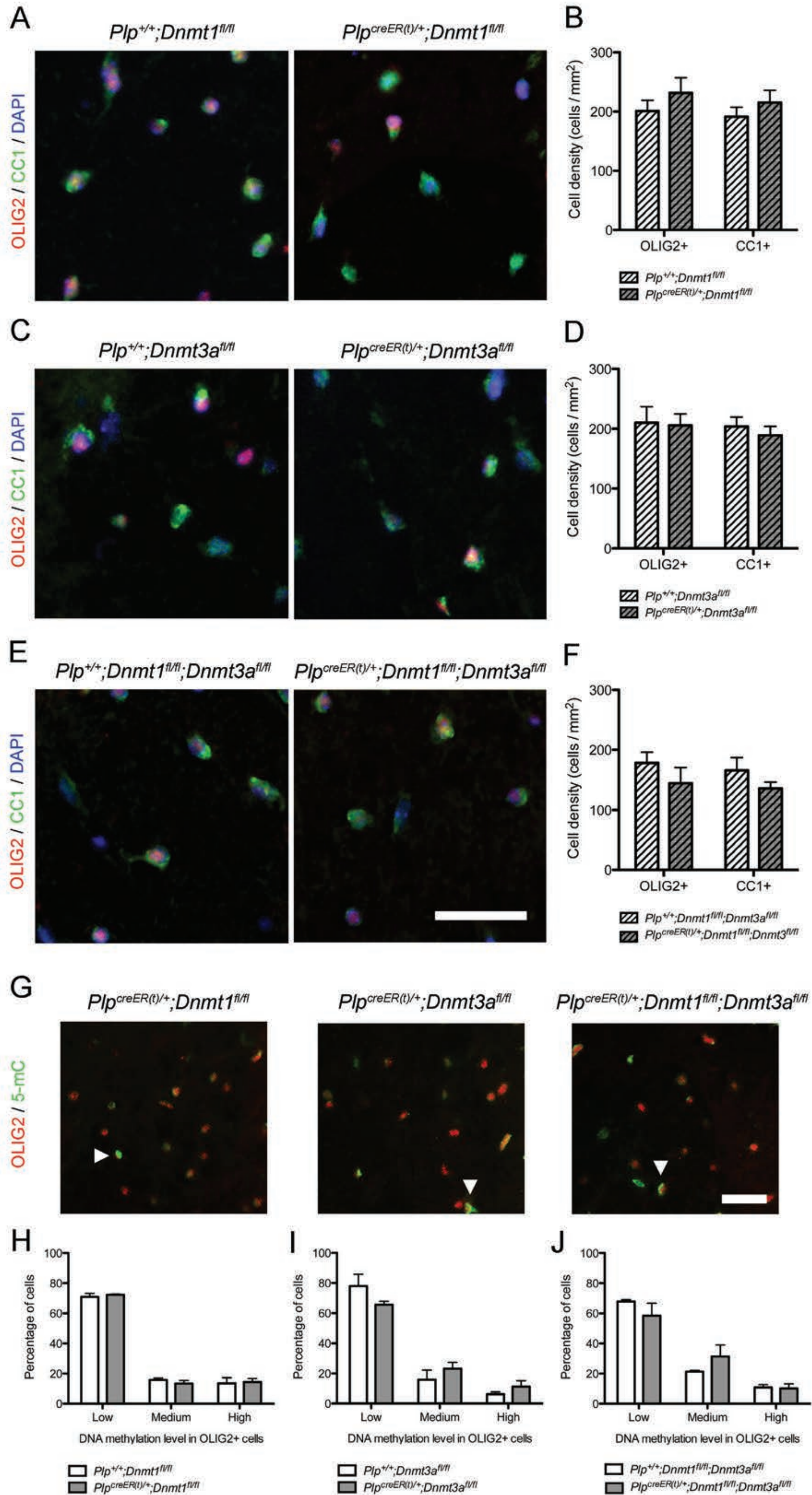

eNeuro Accepted Manuscript

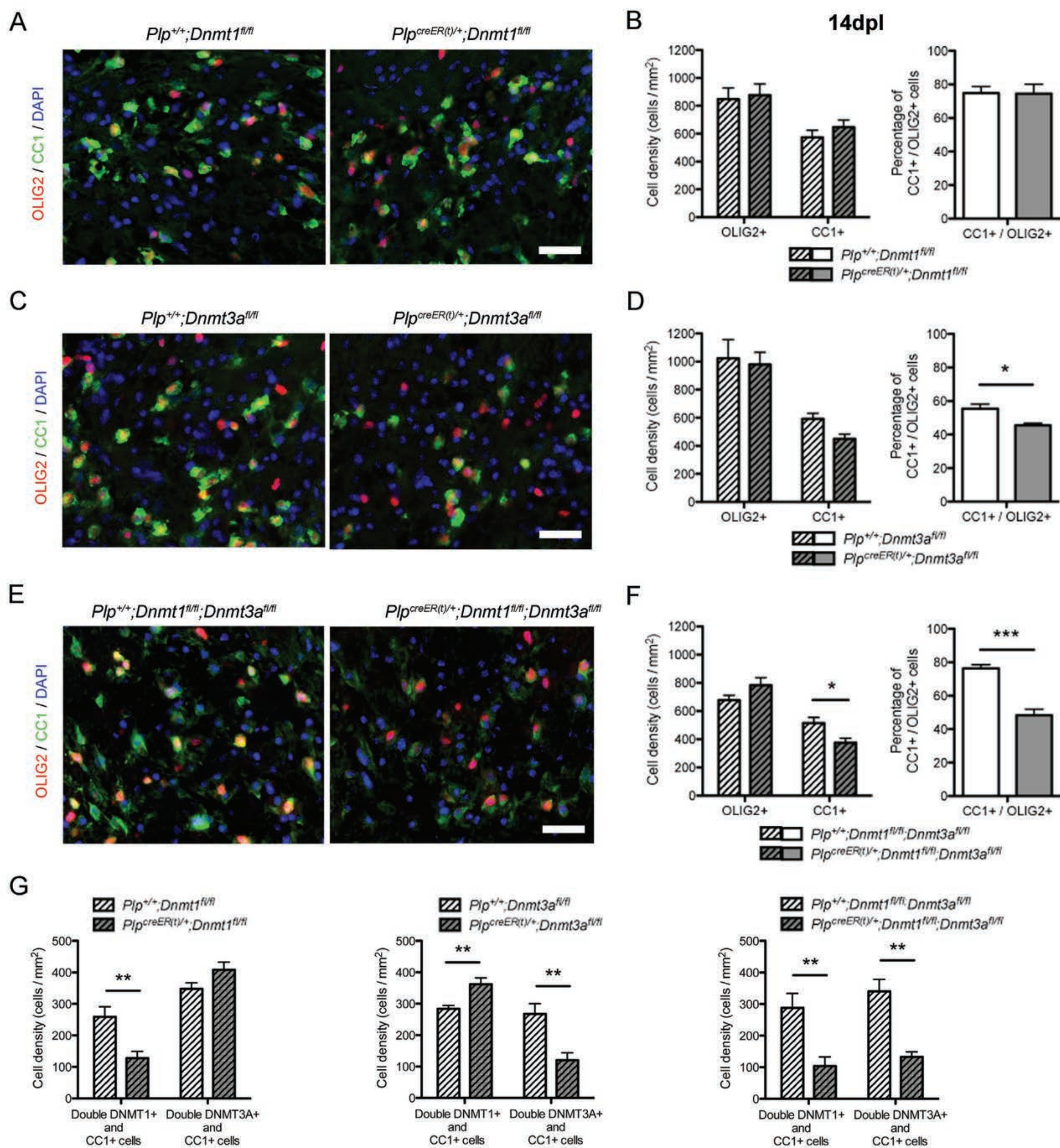

eNeuro Accepted Manuscript

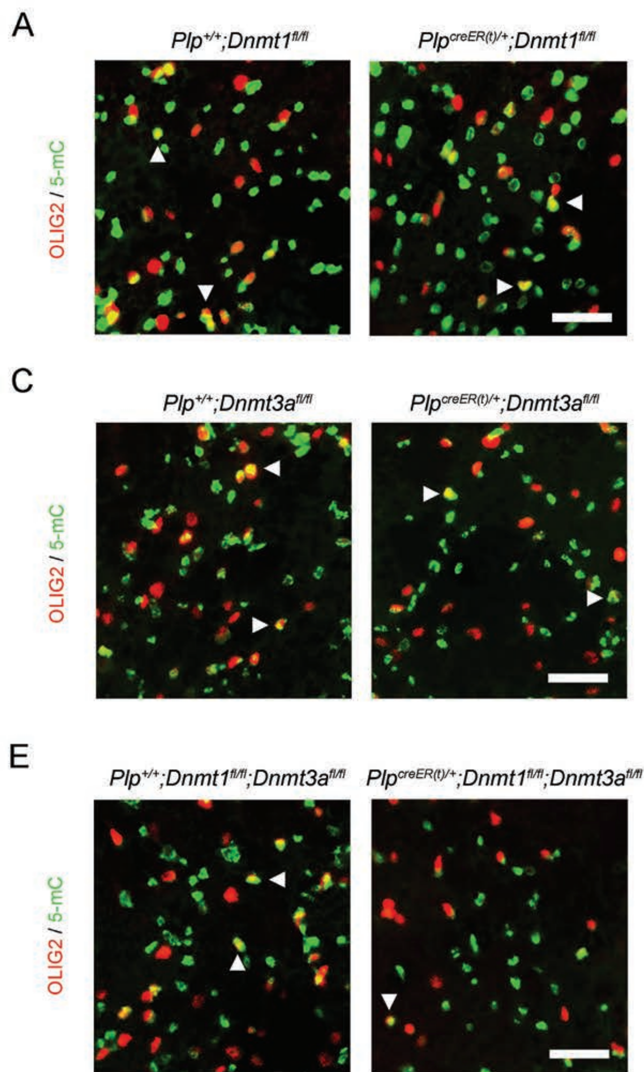

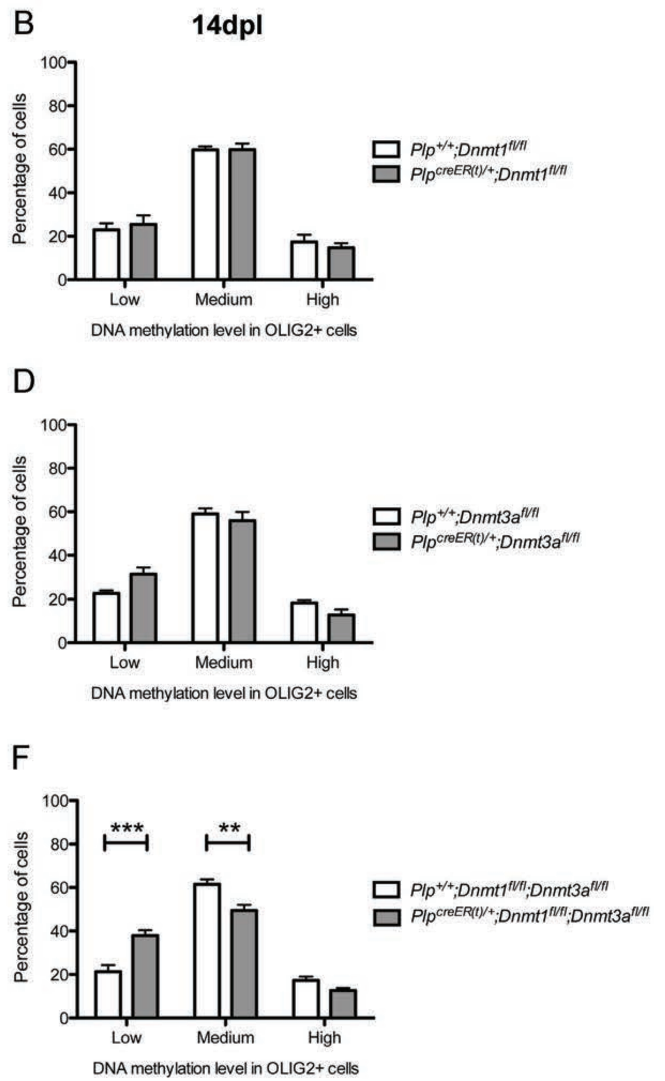

eNeuro Accepted Manuscript